

# Determining the scale of the Bicoid morphogen gradient

Inbal Hecht<sup>1</sup>, Wouter-Jan Rappel, and Herbert Levine

Center for Theoretical Biological Physics and Department of Physics, University of California at San Diego, La Jolla, CA 92093

Edited by José N. Onuchic, University of California San Diego, La Jolla, CA, and approved December 9, 2008 (received for review August 4, 2008)

**Bicoid is a morphogen that sets up the anterior-posterior axis in early *Drosophila* embryos. Although the form of the Bicoid profile is consistent with a simple diffusion/degradation model, the observed length scale is much larger than should be expected based on the measured diffusion rate. Here, we study two possible mechanisms that could, in principle, affect this gradient and, hence, address this disagreement. First, we show that including trapping and release of Bicoid by the nuclei during cleavage cycles does not alter the morphogen length scale. More crucially, the inclusion of advective transport due to cytoplasmic streaming can have a large effect. Specifically, we build a simple model based on the (limited) experimental data and show that such a flow can lead to a Bicoid profile that is consistent with various experimental features. Specifically, the observed length scale is obtained, a steady profile is established, and improved scaling between embryos of different lengths is demonstrated.**

*Drosophila* | embryonic development | flow | length scale

During embryonic development, originally identical cells need to appropriately differentiate into a large variety of cell fates. This differentiation is position-dependent and is regulated by diffusible signaling molecules, known as morphogens. Morphogens are produced in a specific region of a tissue and move away from their source to form long-range concentration gradients. Cells subsequently differentiate in response to the morphogen concentration (1–2); thus, the pattern of morphogen concentration is crucial to the functional formation of tissues and organisms.

In *Drosophila melanogaster*, Bicoid is a maternally transcribed gene that organizes anterior development (3–6). Its mRNA is localized at the anterior pole of the oocyte and is translated shortly after egg deposition. As a consequence of the anterior localization of mRNA, a gradient of Bicoid is formed along the anterior-posterior (AP) axis, simultaneously with nuclear cleavage cycles (7). This gradient determines the boundary of expression of downstream effectors such as Hunchback, eventually leading to the establishment of the segmented body plan. The dynamics of Bicoid pattern formation were recently studied in several experiments (8–15). The gradient was found to have, to a good approximation, an exponential decay with distance from the anterior. The exponential profile is consistent with the general model of diffusion and constant degradation rate which gives a length scale of  $\sqrt{D/\delta}$ , where  $D$  is the diffusion constant and  $\delta$  is the degradation constant.

This simple diffusion/degradation picture, however, turns out to be inconsistent with several recent experiments. In one such experiment (13), the Bicoid diffusion constant was measured using fluorescence measurements of Bicoid-eGFP protein in the nuclei. Upon photobleaching, the recovery rate of nuclear Bicoid was determined, and a diffusion constant of  $D = 0.27 \mu\text{m}^2/\text{s}$  was obtained. With no degradation, this would lead to a length scale of  $\lambda = \sqrt{DT}$  where  $T$  is the time interval during which Bicoid has diffused and  $\lambda$  is the length over which the profile decays from its maximal value (in the production zone) to zero. Performing this calculation for different cycles always lead to length scales that are much smaller than the observed ones. For example, cycle

11 occurs approximately  $T = 90$  min after egg deposition, leading to a length scale of roughly  $38 \mu\text{m}$ . However, experimental results show a much more gradual drop, with a length scale of more than  $60 \mu\text{m}$ , presumably corresponding to a significantly higher diffusion rate.

Some experiments have shown that the Bicoid gradient pattern scales with the length of the embryo (12, 14), a result that is reasonable since each embryo shows the same segmentation pattern. Clearly, patterns arising from simple diffusion with nonvarying diffusivity and degradation are identical in small and large embryos, and a diffusion model is unable to explain the scaling.

In this paper, we present a new model for the Bicoid spreading process, a model that includes cytoplasmic flow. The existence of cytoplasmic fluid flow should be expected based on the motion of the nuclei in the viscous cytoplasm. This nuclear motion consists of two phases with the first one, axial expansion, occurring during division cycles 4–6 and the second one, cortical migration, occurring during cycles 7–9. During axial expansion, the nuclei spread out along the AP axis and are distributed in a hollow ellipsoid in the interior of the embryo (16–17). During the second phase, the nuclei translocate into a uniform monolayer at the cortex. Experiments found that the nuclear velocity during axial expansion was  $23.2 \mu\text{m}/\text{min}$ , whereas during cortical migration it was on average  $7.45 \mu\text{m}/\text{min}$  (17). A study of cytoplasmic fluid flow by Von Dassow and Schubiger (18), however, discovered that the magnitude and spatial dependence of the cytoplasm velocity were not consistent with it being caused directly by viscous drag from the nuclei. Instead, it appears that cytoskeletal forcing drives the flow during these cycles, and rapid flow of the deep cytoplasm from the center of the embryo toward the poles was observed. At the same time, peripheral cytoplasm flows toward the middle region of the embryo, and the waves meet slightly anterior to the middle of the embryo, resulting in a “fountain streaming” pattern. During cycles 1–3, slow, steady movements of the cytoplasm from the poles to the center were observed, corresponding to slow posterior migration of the nuclei.

In this paper, we examine the effect of advection due to this cytoplasmic flow on the Bicoid concentration using computational modeling. We first show that the exchange of Bicoid between the cytoplasm and the nucleus produces nuclear concentration dynamics consistent with experimental data, but does not change the overall length scale of the Bicoid gradient. Then, we show that a reasonable flow pattern, along with fluid velocity comparable to those in ref. 17, lead to length scales that are consistent with the experimentally observed ones for all cycles. Furthermore, we show that the inclusion of cytoplasmic flow can

Author contributions: I.H. and H.L. designed research; I.H. performed research; W.-J.R. contributed new reagents/analytic tools; W.-J.R. and H.L. analyzed data; and I.H., W.-J.R., and H.L. wrote the paper.

The authors declare no conflict of interest.

This article is a PNAS Direct Submission.

<sup>1</sup>To whom correspondence should be addressed. E-mail: inbal.hecht@gmail.com.

© 2009 by The National Academy of Sciences of the USA

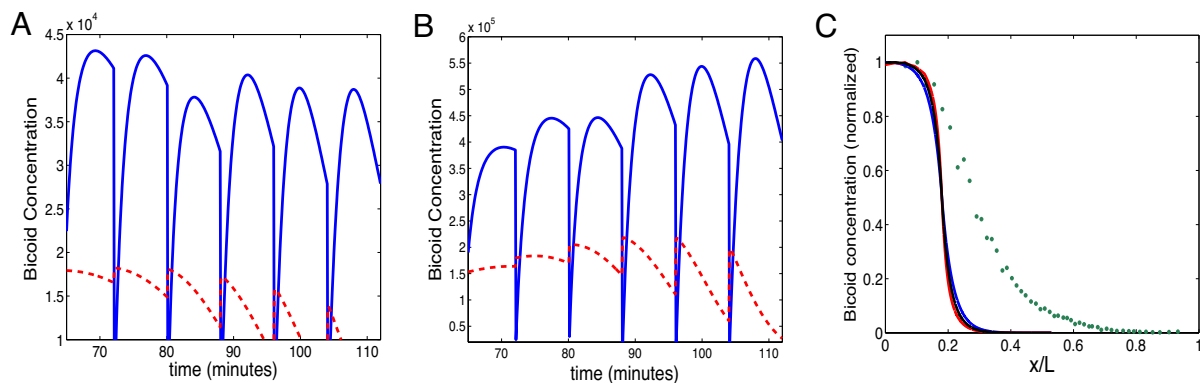


**Fig. 1.** Nuclear trapping model. (A and B) Nuclear Bicoid (solid blue line) and free Bicoid (dashed red line) as a function of time: (A)  $\delta_{free} = 0.001$ ,  $\delta_{nuc} = 0.001$ ; (B)  $\delta_{free} = 0$ ,  $\delta_{nuc} = 0.001$ . (C) Normalized concentration of Bicoid in a cycle 12 embryo: free Bicoid for diffusion-only model (blue line), free Bicoid for the nuclear dynamics model (red line), nuclear Bicoid (asterisks), and experimental results from the FlyEx database (24–27) (circles).

explain the observed scaling of the pattern. Our predictions should be testable in experiments that measure the flow pattern and flow velocity.

## Results

We first investigated the role played by the nuclei in the formation of the Bicoid gradient pattern using a simple one dimensional (1D) model (see *Methods*). We implemented coupling between a cytoplasmic space, representing the entire cross-section perpendicular to the AP axis, and finite nuclear compartments. The rate at which the nuclei trap the cytoplasmic Bicoid was chosen to reproduce experimental observations. A too high binding rate leads to fast depletion of Bicoid and to a sharp decrease in the nuclear Bicoid concentration, whereas a too low binding rate leads to a free Bicoid/nuclear Bicoid ratio that is too high compared to the experimental results.

The nuclei grow synchronously at a constant rate and divide when their radii exceed a critical value (mitosis). During mitosis the nuclear envelope breaks down, and all Bicoid is released into the bulk. Cytoplasmic Bicoid diffuses along the 1D line with a diffusion constant of  $D = 0.3 \mu\text{m}^2/\text{s}$ , and both the nuclear and cytoplasmic Bicoid degradation are included in the model. The maximal radius of each nucleus is taken to be  $5 \mu\text{m}$  up to cycle 10 and then 5.25, 4.6, 4.1, and  $3.25 \mu\text{m}$  during cycles 11–14, respectively (19).

In Fig. 1A, we show the concentration inside the nucleus that is  $\approx 125 \mu\text{m}$  from the anterior pole, along with the cytoplasmic concentration at that location. Similar to experiments, the nuclear concentration during each cycle shows an increase followed by a decrease. The increasing phase of the nuclear concentration is due to the flux from the cytoplasm into the nucleus. In addition to the nuclear degradation, the decrease stems from the fact that the volume of a growing sphere is changing faster ( $\approx R^3$ ) than the flux ( $\approx R$ ). Our simulation results also agree with another key experimental finding, namely that the peak nuclear concentration remains roughly constant in subsequent cycles. For this to occur, two conditions need to be met. First, the free Bicoid profile needs to reach steady state, namely there is a significant degradation of the free Bicoid. This is needed because the change of the nuclear radius during cycles 9–12 is relatively small. Second, the nuclear degradation rate has to roughly match the change in the nuclear size in such a way that the concentration (and not the overall Bicoid amount) will remain constant. This nuclear degradation is insufficient and cannot yield a constant concentration when the number of nuclei is small, at least up to cycle 10. Therefore, in order for concentration peaks to be roughly constant during cycles 9–14, free Bicoid degradation is needed and the nuclear degradation

cannot dominate, in disagreement with the model suggested by Gregor *et al.* (13). Bergmann *et al.* (19) argued that a constant free Bicoid concentration, together with a decreasing nuclear size, will result in an increasing nuclear Bicoid concentration. However, this argument does not take into account the depletion effect, which becomes significant as the number of nuclei becomes high. This can be seen in Fig. 1A and B, where the drop in the free Bicoid concentration becomes larger from cycle to cycle. We show here that a constant free Bicoid concentration (namely its peak values) and an increasing nuclear size may result in a constant nuclear concentration, given the correct parameter values. It should also be noted that taking into account Bicoid mRNA degradation starting at cycle 12 (simply by adjusting the production rate) will demand the tuning of the parameters but may lead to qualitatively similar results (data not shown).

The corresponding normalized cytoplasmic Bicoid concentration profile is shown in Fig. 1C with and without nuclear trapping. Even though the inclusion of nuclear trapping can alter the magnitude of the cytoplasmic Bicoid concentration significantly, it leaves the length scale of the Bicoid concentration virtually unchanged. It should be noted that this applies to the range of parameters in which constant peak values are achieved and the ratio between free and nuclear Bicoid is similar to the experimental one. Other cases, such as stronger binding in the nuclei or stronger nuclear degradation, may result in slower diffusion and, therefore, in a smaller length scale. To compare the profile obtained from our simple diffusion model with experiments, we have also plotted a profile obtained from the FlyEx database (25–28). This comparison shows that the length scale obtained using the simple diffusion and degradation model is much smaller than the experimentally observed one.

To address this inconsistency, we next studied the role of cytoplasmic streaming on the formation of the gradient. This was done in a two-dimensional (2D) elliptical cell model in which the molecular motion due to diffusion is augmented by additional advection during cycles 4–6 (see *Methods*). Nuclear dynamics is neglected because it does not affect the length scale of the profile, as shown above. During all cycles, Bicoid is produced in a zone adjacent to the anterior pole. Instead of directly modeling the flow equations and their cytoskeletal driving, we adopted a phenomenological approach and used a measured pattern with a fixed flow speed. The “fountain streaming” flow pattern, shown in Fig. 2A, is added to the diffusion process. A “cortical migration” pattern during cycles 7–9 was found to have negligible effect on the profile (data not shown) and was omitted. To reliably compare our results with the experimental data, we used the same method for Bicoid concentration visualization as in experiments. This method measures the Bicoid concentration



this case, the positional error is even larger and is  $\approx 3.3\%$  embryo length for that region. We can obtain improved scaling, however, if we assume that the “fountain streaming” magnitude scales with the embryo length. This is shown in Fig. 3C where the flow velocity in the larger embryo is increased by a factor equal to the ratio of the embryo lengths. Now, we find that the positional error is  $\approx 1\%$  on average, and even smaller for the half-maximal point.

## Discussion

The prime motivation for this study was to offer an explanation for the experimentally determined length scales of the Bicoid gradient. These length scales, as observed by many groups, are incompatible with a simple diffusive process using the experimentally measured diffusion constant and given the relevant time. Thus, another mechanism is likely to be involved in the formation of these gradients, and we show that cytoplasmic fluid flow during cycles 4–6 is able to produce experimentally observed length scales during cycles 10–14. This fluid flow has been observed experimentally and is most likely to result from membrane contractions, caused by cortical recruitment of myosin-II just above the nuclear cloud (20–23). This recruitment is possible only during interphase, when the Cdc2 level is low and, therefore, myosin-II is not inhibited. Cortical myosin is first seen at cycle 4, in a patch at the antero-central part of the embryo at  $\approx 1/3$  egg length from the anterior. A cortical contraction accompanies each cycle of myosin accumulation, leading to the motion of the nuclei along the AP axis. With each succeeding cycle, the patch expands poleward, dispersing at the beginning of each mitosis and reassembling at the end of telophase (23). These contractions cause cytoplasmic streaming which carries the nuclei along the AP axis. Although the contractions may seem bidirectional, the motion of the nuclei indicates that there is a net poleward flow. The possibility that other processes, such as cytoplasmic contractions, may play a role in morphogen gradient formation was raised by Driever and Nusslein-Volhard (3) but has not been quantitatively studied to date. We should note that a direct measurement of the diffusion constant using injected inert Dextran particles yielded a much higher diffusion coefficient ( $13\text{--}30 \mu\text{m}^2/\text{s}$ ) than the diffusion coefficient of Bicoid. It has been suggested that this high diffusion constant is brought about by stirring due to cytoplasmic flow (13), again demonstrating the possible effect of net fluid flow. In this work, we not only assess the role of such a flow, but also suggest the putative mechanism that brings about a directional advective motion of the morphogen, based on the known experimental data.

Using computer simulations, we find that for our flow pattern, fluid velocity of  $\approx 0.08 \mu\text{m}/\text{s}$  can change the profile significantly and can produce experimentally observed length scales. This fluid speed is consistent with a rough estimate of the effect of advection. We expect that our main conclusion, that cytoplasmic flow can produce Bicoid gradients with experimentally observed length scales, to be largely independent of the details of the flow pattern. In fact, the only requirement is a net transport along the cortex from the anterior pole toward the midpoint of the embryo. Of course, this prediction requires an experimental validation.

We also showed, using a simple 1D model, that the exchange between the nuclei and the cytoplasm does not affect the length scale characteristics of the Bicoid profile, within the range of parameters that fits the experimental observations. This result can be compared to a recent study by Coppey *et al.* (24) which also studied the role of nuclear Bicoid trapping in a 1D model. Their model did not explicitly consider discrete nuclei, but they also found that the shape of the gradient is unaffected by nuclear trapping. We also found that, as long as the nuclear trapping rate is not too high, it is possible to obtain peak nuclear concentrations that are roughly constant between cycles. We showed that

this trapping rate can be chosen such that the ratio of the peak nuclear concentration and the cytoplasmic Bicoid concentration correspond with the experimental value.

Bergmann *et al.* (15) discussed the role of pre-steady state decoding of the Bicoid profile. In this work, we do not refer to downstream genes, but would like to note that from both experimental works of Bergmann *et al.* (15) and Gregor *et al.* (13) it seems that the Bicoid profile does not change significantly after cycle 11 or 12. In our flow model, a nearly steady profile is obtained for this time frame, independent of the degradation rate. Due to the advection, the profile changes quickly in early cycles, and when advection is no longer present, it remains steady by diffusion. Our model can, therefore, explain how a large length scale and a steady profile are achieved with slow diffusion and relatively short time.

A number of experiments have shown that the Bicoid profile scales with the embryo length, as embryos of various sizes and of various species have the same body proportions (12, 14). Other experiments (8) have shown that Bicoid profiles within the same species do not scale, and only Hunchback and other downstream effectors scale with the embryo length. However, it was recently argued by Gregor *et al.* (14) that the normalization method used in ref. 8 actually imposed the obtained variance of the Bicoid profiles. Gregor *et al.* (14) showed that raw data of BCD-GFP, or data with one global calibration, exhibit reproducibility in different embryos. Although further experimental research is needed, we assume that scaling of the Bicoid profile with the embryo length is a required feature of any model. Several possibilities for the mechanism producing this scaling have been proposed, including oppositely directed morphogen gradients (29–30), RNA-binding proteins (31), or nuclear degradation (13). Our flow model can improve scaling provided that the flow magnitude also scales with the embryo length. This assumption is perhaps reasonable, as the flow is produced by the contractions resulting from a myosin patch. If the myosin patch size scales with the embryo size, then one should expect the contraction strength, and therefore, the flow velocity, to scale with the embryo size as well.

There are other, more general aspects of morphogen pattern formation that need to be studied in light of the suggested flow model. For example, the effect of Bicoid dosage change on the pattern of downstream effectors (15) may or may not depend on the characteristics of the flow pattern. The model suggested here is based on linear diffusion and advection, and therefore, a change in Bicoid dosage will result in a corresponding linear change in the pattern. Downstream effectors will then be influenced according to the specific characteristics of their network (15). Another example is temperature dependence of the flow magnitude. Higher incubation temperatures result in faster nuclear cycles but eventually lead to a normal embryo (30). This may be related to enhanced advection that results from stronger or faster myosin contractions. In a recent study, Lucchetta *et al.* (32) found that a temperature gradient along the embryo can induce cytoplasmic flow. This interesting phenomenon was discovered using differential interference contrast (DIC) microscopy together with image analysis software that traced “particles” in the cytoplasm. It should be possible to apply a similar method to the study of fountain streaming to obtain both qualitative and quantitative description of the cytoplasmic flow and of the resulting Bicoid spreading process.

Our model is admittedly schematic, a necessity in view of the limited amount of available data. It hopefully will lead to new experiments that probe the detailed properties of cytoplasmic flow. For example, the exact flow pattern is unknown but could be determined experimentally. Furthermore, we assume, lacking precise experimental data, that the fluid speed is uniform. Clearly, this is not likely to be the case experimentally, and a fluid flow map needs to be determined. The good agreement between our simulations and experimental data were based on several

fitting parameters, especially including the magnitude of the flow velocity. Hence, this magnitude should be viewed as a prediction to be tested in future studies.

## Methods

For the nuclear dynamics model, we used a 1D model of the embryo cortex, with no-flux boundary conditions at either end. As explained above, this 1D representation of the embryo is a projection onto the AP axis which is taken to be 500  $\mu\text{m}$  long. The line is discretized using a discretization parameter,  $\Delta x$ , and a zone of constant Bicoid production extends 90  $\mu\text{m}$  from the anterior pole (production rate  $p_0 = 300 \text{ s}^{-1}$ ). Cytoplasmic Bicoid diffuses with  $D = 0.3 \mu\text{m}^2/\text{s}$  [as measured by Gregor *et al.* (13)] and degrades with degradation constant  $\delta_{\text{free}}$ . Nuclei are positioned at  $x_n$  and are modeled as point particles with a size  $R(t)$ . There is initially one nucleus with radius  $R_{\text{min}} = 2 \mu\text{m}$ , positioned at the anterior pole, which grows constantly until  $R_{\text{max}} = 4.5 \mu\text{m}$ , after which it splits into two nuclei, each with a radius  $R_{\text{min}} = 2 \mu\text{m}$ . The positions of the two new nuclei are chosen as follows: one is placed at the original position and one is positioned halfway between the original position and its nearest neighbor, with the posterior pole functioning as the location of the neighbor for the nucleus furthest removed from the anterior. Nuclear motion was not taken into account in our simulations. The concentration of Bicoid in the nucleus is determined by the flux of free Bicoid  $k_{\text{in}}$  into the nucleus and by the nuclear degradation rate  $\delta_{\text{nuc}}$ . The equations for the concentration of free Bicoid ( $B_{\text{free}}$ ) and the total amount of nuclear Bicoid ( $B_{\text{nuc}}$ ) are thus:

$$\frac{dB_{\text{free}}}{dt} = D\nabla^2 B_{\text{free}} - \delta_{\text{free}}B_{\text{free}} - \frac{k_{\text{in}}B_{\text{free}}}{A}\delta(x - x_n) \quad [1]$$

$$\frac{dB_{\text{nuc}}}{dt} = k_{\text{in}}B_{\text{free}} - \delta_{\text{nuc}}B_{\text{nuc}} \quad [2]$$

In ref. 13, the suggested formula for  $k_{\text{in}}$  was  $k_{\text{in}} = 4\pi RD$ . This corresponds to the case of perfect binding -fully absorbing nuclei. However, this assumption is not consistent with other experimental findings such as the ratio between free and nuclear Bicoid and the steady peak values of nuclear Bicoid concentration during the late cycles. To introduce nonperfect binding sites, one should use the boundary condition:

$$D\frac{\partial C}{\partial r}\Big|_{r=R} - \alpha C = 0 \quad [3]$$

with  $\alpha = 0$  for a fully reflective boundary and  $\alpha \rightarrow \infty$  for a fully absorbing one. Solving for  $C$  and taking the flux one obtains

$$f = 4\pi R^2 D \frac{\partial C}{\partial r}\Big|_{r=R}$$

$$k_{\text{in}} = \frac{4\pi R^2 D \alpha}{D + R\alpha} \quad [4]$$

for any  $\alpha$  in the range  $[0, \infty)$ . A high value of  $\alpha$  yields a sharp decrease in the nuclear Bicoid concentration during later cycles, due to the depletion of free Bicoid and the enhanced nuclear degradation. A low value of  $\alpha$  yields a high free/nuclear Bicoid ratio. To balance these two effects, we chose  $\alpha = 0.025$ , which gives a free/nuclear Bicoid concentration ratio as obtained in the experiments together with a moderate decrease in the concentration.

Eq. 1 is discretized in the following way:

$$\frac{\Delta B_{\text{free}}}{\Delta t} = D\nabla^2 B_{\text{free}} - \delta_{\text{free}}B_{\text{free}} - \frac{k_{\text{in}}B_{\text{free}}}{A\Delta x}\delta_{x,x_n} \quad [5]$$

Here,  $A\Delta x$  is a geometric factor arising from the projection onto the AP axis. For simplicity, the area of the cross section of the embryo,  $A$ , is chosen to be constant throughout the embryo. Simulations in which this area was chosen to be a function of the distance along the AP axis gave similar qualitative results outside the production zone (data not shown). Finally, at the end of each cycle, of duration 8 min, mitosis is modeled by adding the nuclear Bicoid to the cytoplasmic concentration and resetting the nuclear concentration to zero.

Flow simulations were performed on a 2D rectangular lattice, using an elliptical embryo with axes of 180 and 500  $\mu\text{m}$ , and with zero normal flux along its boundaries. As in the 1D calculation, every cycle was assumed to last 8 min. The equation describing the Bicoid dynamics includes production, degradation, and diffusion according to the following equation:

$$\frac{dB}{dt} = P(x) + D\nabla^2 B - \delta B - \vec{v}_{\text{flow}}(x, y) \cdot \vec{\nabla} B \quad [6]$$

where  $B$  is Bicoid concentration,  $D = 0.3 \mu\text{m}^2/\text{s}$  is the diffusion constant,  $\delta$  is the degradation rate, and  $P(x)$  is the production function encompassing the 18% of the embryo closest to the anterior pole, in accordance with experimental evidence (3, 8, 25–28). The production rate  $p_0 = 100 \text{ s}^{-1}$  is kept constant through all cycles. Nuclear dynamics, i.e., the flux of Bicoid in and out of the nuclei, was ignored.

The last term in this equation describes the coupling of the diffusion to the fluid flow where  $\vec{v}_{\text{flow}}$  is the fluid velocity. This fluid velocity was chosen to be zero in cycles 1–3 and for 7–14. The flow field for the fountain streaming, during cycles 4–6, was created using Matlab and its PDE toolbox. This “fountain streaming” pattern is shown in Fig. 2A. Because we had no accurate data about the speed during fountain streaming and no knowledge about either the speed distribution along the embryo or the effect of reverse flow, we chose the velocity magnitude to be uniform within the embryo. This is inspired by the experiments showing large scale fluid flow near the poles as well as in the center of the embryo. Trying to estimate the flow magnitude was more difficult; the results of Baker *et al.* (17) show a large diversity of nuclear motion velocities between 0.02  $\mu\text{m}/\text{s}$  and 0.4  $\mu\text{m}/\text{s}$ , varying between the different cycles and different sides of the embryo. We used an averaged magnitude of the fluid flow of 0.08  $\mu\text{m}/\text{s}$ , which showed good agreement with the experimental profiles. Further experiments are needed to have a more accurate estimate. The chosen velocity field indicates a volume change during the “fountain streaming” phase, as  $\text{div } \vec{v} \neq 0$ . For the chosen magnitude, the velocity field yields a volume change of  $\approx 15\%$ , which seems reasonable compared to experimental movies.

To compare our simulation results with experiments we used an averaging box of size 10  $\mu\text{m} \times 10 \mu\text{m}$ , sliding along the egg cortex, to detect the concentration of Bicoid at every point (compare to that in ref. 13). This was done using custom software in Matlab. The averaged value was then projected onto the AP axis. Experimental data from the FlyEx database (25–28) was also averaged over approximately 10- $\mu\text{m}$  intervals. The presented data of embryos at different stages refer to different embryos but embryo-to-embryo variability is low.

**ACKNOWLEDGMENTS.** We thank Thomas Gregor for useful discussions and inspiring experimental data. This work was supported by the Center for Theoretical Biological Physics (National Science Foundation PHY-0822283).

- Lawrence PA, Struhl G (1996) Morphogens, compartments, and pattern: lessons from *Drosophila*. *Cell* 85:951–961.
- Gurdon JB, Bourillot PY (2001) Morphogen gradient interpretation. *Nature* 413:797–803.
- Driever W, Nusslein-Volhard C (1988) A gradient of Bicoid protein in *Drosophila* embryos. *Cell* 54:83–93.
- Driever W, Nusslein-Volhard C (1988) The Bicoid protein determines position in the *Drosophila* embryo. *Cell* 54:95–104.
- Driever W (1993) in *The development of Drosophila Melanogaster*, eds Bate M, Ariaz AM (Cold Spring Harbor Laboratory Press, Cold Spring Harbor, NY).
- Jaeger J, *et al.* (2004) Dynamic control of positional information in the early *Drosophila* embryo. *Nature* 430:368–371.
- Foe VE, Odell GM, Edgar BA (1993), in *The development of Drosophila Melanogaster*, eds Bate M, Ariaz AM (Cold Spring Harbor Laboratory, Cold Spring Harbor, NY).
- Houchmandzadeh B, Wieschaus E, Leibler S (2002) Establishment of developmental precision and proportions in the early *Drosophila* embryo. *Nature* 415:798–802.
- Houchmandzadeh B, Wieschaus E, Leibler S (2005) Precise domain specification in the developing *Drosophila* embryo. *Phys Rev E* 72:061920.
- Lebrecht D, *et al.* (2005) Bicoid cooperative DNA binding is critical for embryonic patterning in *Drosophila*. *Proc Natl Acad Sci USA* 102:13176–13181.
- Crauk O, Dostalni N (2005) Bicoid Determines Sharp and Precise Target Gene Expression in the *Drosophila* Embryo. *Curr Biol* 15:1888–1898.
- Gregor T, Bialek W, de Ruyter van Steveninck RR, Tank DW, Wieschaus EF (2005) Diffusion and scaling during early embryonic pattern formation. *Proc Natl Acad Sci USA* 102:18403–18407.
- Gregor T, Wieschaus EF, McGregor AP, Bialek W, Tank DW (2007) Stability and nuclear dynamics of the Bicoid morphogen gradient. *Cell* 130:141–152.
- Gregor T, Tank DW, Wieschaus EF, Bialek W (2007) Probing the limits to positional information. *Cell* 130:153–164.
- Bergmann S, *et al.* (2007) Pre-steady state decoding of the Bicoid morphogen gradient. *PLoS Biol* 5:232.
- Sullivan W, Theurkauf WE (1995) The cytoskeleton and morphogenesis of the early *Drosophila* embryo. *Curr Opin Cell Biol* 7:18–22.
- Baker J, Theurkauf WE, Sehubiger G (1993) Dynamic changes in microtubule configuration correlate with nuclear migration in the preblastoderm *Drosophila* embryo. *J Cell Biol* 122:113–121.

18. von Dassow G, Schubiger G (1994) How an actin network might cause fountain streaming and nuclear migration in the syncytial *Drosophila* embryo. *J Cell Biol* 127:1637–1653.
19. Bergmann S, Tamari Z, Schejter E, Shilo BZ, Barkai N (2008) Re-examining the stability of the Bicoid morphogen gradient. *Cell* 132:15–17.
20. Hatanaka K, Okada M (1991) Retarded nuclear migration in *Drosophila* embryos with aberrant F-actin reorganization caused by maternal mutations and by cytochalasin treatment. *Development* 111:909–920.
21. Hatanaka K, Okada M (1991) Mutations affecting embryonic F-actin reorganization also affect separation of nuclei from their sisters and from the cortex in *Drosophila* cleavage embryos. *Develop Growth Differ* 33:535–542.
22. Wheatley S, Kulkarni S, Karess R (1995) *Drosophila* nonmuscle myosin II is required for rapid cytoplasmic transport during oogenesis and for axial nuclear migration in early embryos. *Development* 121:1937–1946.
23. Royou A, Sullivan W, Karess R (2002) Cortical recruitment of nonmuscle myosin II in early syncytial *Drosophila* embryos: its role in nuclear axial expansion and its regulation by Cdc2 activity. *J Cell Biol* 158:127–137.
24. Coppey M, Berezhkovskii AM, Kim Y, Boettiger AN, Shvartsman SY (2007) Modeling the bicoid gradient: Diffusion and reversible nuclear trapping of a stable protein. *Develop Biol* 312:623–630.
25. Poustelnikova E, Pisarev A, Blagov M, Samsonova M, Reinitz J (2004) A database for management of gene expression data in situ. *Bioinformatics* 20:2212–2221.
26. Kosman D, Reinitz J, Sharp DH (1998) Automated assay of gene expression at cellular resolution. In *Proceedings of the 1998 Pacific Symposium on Biocomputing*, eds Altman R, Dunker K, Hunter L, Klein T (World Scientific, Singapore), pp 6–17.
27. Kosman D, Small S, Reinitz J (1998) Rapid preparation of a panel of polyclonal antibodies to *Drosophila* segmentation proteins. *Dev Genes Evol* 208:290–294.
28. Surkova S, et al. (2008) Characterization of the *Drosophila* segment determination morphome. *Develop Biol* 313:844–862.
29. McHale P, Rappel WJ, Levine H (2006) Embryonic pattern scaling achieved by oppositely directed morphogen gradients. *Phys Biol* 3:107–120.
30. Lucchetta EM, Lee JH, Fu LA, Pate NH, Ismagilov RF (2005) Dynamics of *Drosophila* embryonic patterning network perturbed in space and time using microfluidics. *Nature* 434:1134–1138.
31. Aegerter-Wilmsen T, Aegerter CM, Bisseling T (2005) Model for the robust establishment of precise proportions in the early *Drosophila* embryo. *J Theor Biol* 234:13–19.
32. Lucchetta EM, Vincent ME, Ismagilov RF (2008) A precise Bicoid gradient is nonessential during cycles 11–13 for precise patterning in the *Drosophila* blastoderm. *PLoS ONE* 3: e3651.